An Artificial Miniaturized Peroxidase for Signal Amplification in Lateral Flow Immunoassays

Emilia Renzi, Andrew Piper, Flavia Nastri, Arben Merkoçi,* and Angela Lombardi*

Signal amplification strategies are widely used for improving the sensitivity of lateral flow immunoassays (LFiAs). Herein, the artificial miniaturized peroxidase Fe(III)-MimochromeVI*a (FeMC6*a), immobilized on gold nanoparticles (AuNPs), is used as a strategy to obtain catalytic signal amplification in sandwich immunoassays on lateral flow strips. The assay scheme uses AuNPs decorated with the mini-peroxidase FeMC6*a and anti-human-IgG as a detection antibody (dAb), for the detection of human-IgG, as a model analyte. Recognition of the analyte by the capture and detection antibodies is first evidenced by the appearance of a red color in the test line (TL), due to the accumulation of AuNPs. Subsequent addition of 3,3′,5,5′-tetramethylbenzidine (TMB) induces an increase of the test line color, due to the TMB being converted into an insoluble colored product, catalyzed by FeMC6*a. This work shows that FeMC6*a acts as an efficient catalyst in paper, increasing the sensitivity of an LFiA up to four times with respect to a conventional LFiA. Furthermore, FeMC6*a achieves lower limits of detection that are found in control experiments where it is replaced with horseradish peroxidase (HRP), its natural counterpart. This study represents a significant proof-of-concept for the development of more sensitive LFiAs, for different analytes, based on properly designed artificial metalloenzymes.

1. Introduction

Paper-based biosensors, in particular lateral flow assays (LFAs), are commonly used around the world since they are inexpensive, fast, simple to use and interpret, robust, reliable,

E. Renzi, F. Nastri, A. Lombardi
Department of Chemical Sciences
University of Napoli Federico II
Via Cintia, 21, Napoli 80126, Italy
E-mail: alombard@unina.it

E. Renzi, A. Piper, A. Merkoçi
Nanobioelectronics & Biosensors Group
Institut Català de Nanociència I Nanotecnologia (ICN2)
CSIC and The Barcelona Institute of Science and Technology (BIST)
Campus UAB, Bellaterra, Barcelona 08193, Spain
E-mail: arben.merkoci@icn2.cat

A. Merkoçi
Catalan Institution for Research and Advanced Studies (ICREA)
Pg. Lluís Companys 23, Barcelona 08010, Spain

The ORCID identification number(s) for the author(s) of this article can be found under https://doi.org/10.1002/smll.202207949.

sensitive and specific. In this sense, LFAs satisfy all the criteria required for ideal point-of-care devices (POCDs).[1–3] When antibodies are exploited as biorecognition elements, LFAs are categorized as "lateral flow immunoassays (LFiAs)". LFiAs are manufactured as strips with four component parts: the sample pad, where the sample solution is added to the strip; the conjugate pad, where the detection antibodies (dAbs), amongst other things, are stored; a nitrocellulose membrane, onto which antibodies are printed to create a test line (TL) and a control line (CL); an absorbent pad, which enhances the flow and adsorbs the excess solution flowing laterally along the strip.[3] The pads need to be in direct contact with each other to allow the sample solution to flow through them, driven solely by capillary force until wicking.[4] When the output of the assay is a colorimetric signal, nanoparticles are often used (because of their high surface-to-volume ratio) to concentrate multiple copies of the dAbs on a small surface.[5,6]

At the time of writing, gold nanoparticles (AuNPs) are commonly used for this application. AuNPs are popular because they offer a variety of surface functionalization protocols, can be easily and reproducibly synthesized in a variety of shapes and sizes, are colloidally stable, and produce a strong red color (when 20 nm in diameter, as it is most commonly used) which is ideal for the naked eye detection.[7,8] The working principle of an LFiA is exhaustively reported in the literature.[4,9,10] In brief, considering an immune-sandwich assay, when the sample solution is introduced to the sample pad, the analyte (in the case of a positive sample) binds to the detection antibody on the AuNPs and this conjugate flows through the nitrocellulose in the direction of the absorbent pad. When it reaches the TL and CL, the AuNP/dAb/analyte complex binds to the capture antibodies printed in these lines and the accumulation of AuNPs gives rise to a red color. The capture antibodies in the TL will only bind to the AuNP/dAb/analyte complex, whereas those in the CL will bind to the AuNP/dAb conjugate, to affirm that the solution has wicked the full distance of the strip and that the strip has been prepared properly. The intensity of the red color in the TL should be directly proportional to the concentration of analyte in the sample solution being tested.[11] With the use of a proper LFA reader, it is possible to estimate the concentration of the analyte in the sample solution and determine the limit of detection and sensitivity of the developed assay.[12–14]

ADVANCED
SCIENCE NEWS
www.advancedsciencenews.com

NANO · MICRO
small
www.small-journal.com

This working principle has been used to develop LFiAs for multiple diagnostic applications, including pregnancy tests,[15] COVID-19 antigen tests,[16–18] as well as for safety and environmental analyses.[19,20]

Despite their many advantages, the LFiAs lack the sensitivity required to detect many desirable biomarkers, which currently have to be detected with laboratory assays.[21,22] Recent studies have therefore focused on developing signal enhancement strategies.[23–26] There are too many of these works to discuss in detail here, but some notable methodologies include: enlargement of the particle size by silver coating,[27] coating the AuNPs with a catalytic metal,[28,29] varying the geometry of the LFiA components,[30] engineering core-shell multifunctional AuNPs,[31] and tuning the flow rate using wax barriers.[32,33] Also, many efforts have been devoted to achieving signal amplification with enzyme-catalyzed chemical reactions,[34] exploiting the activity of enzymes on AuNP surfaces to convert substrates into colored products. For instance, horseradish peroxidase (HRP) catalyzes the oxidation of colorless 3,3′,5,5′-tetramethylbenzidine (TMB) to create a blue-colored product. The generation of a color localized at the TL has been shown to significantly enhance the sensitivity of the assay.[35]

The suitability of enzymes to catalyze the conversion of chromogenic substrates into colored products, for the purpose of enhancing LFA sensitivity, is well established.[34] However, the use of natural enzymes suffers from severe drawbacks, such as low stability, loss of activity, and denaturation over long storage times. Thus, many efforts are being devoted to developing artificial enzymes for several applications.[36–40] Among artificial metalloenzymes, Mimochromes (MCs) were conceived by us as mimics of natural heme-proteins and developed using a miniaturization approach followed by iterative re-design steps.[37,41,42] MCs are composed of two small helical peptide chains covalently linked to the propionic groups of a deuteroporphyrin IX (DPIX). After several rounds of re-design, shaping both first- and second-coordination shell interactions[43] and conformational constraints,[44] Mimochrome VI*a (MC6*a) was identified as the best scaffold for catalytic purposes.

MC6*a can host several metal ions, affording artificial enzymes with a tailored catalytic activity.[45–48] In its Fe(III) complex, MC6*a acts as a robust and highly active peroxidase (**Figure 1**A), displaying a 20-fold higher catalytic efficiency in 2,2′-azino-bis(3-ethylbenzothiazoline-6-sulfonic acid (ABTS) oxidation than that of wild-type HRP.[44] Despite its simplified structure, experimental data have proven the ability of FeMC6*a to outperform natural and artificial biocatalysts in catalyzing several oxidation reactions.[49,50] The success of this approach has paved the way to further widen the functional repertoire of FeMC6*a, exploring its catalytic potential after conjugation on gold electrodes and nanomaterials.[51,52] Since FeMC6*a retains its structure and catalytic behavior when conjugated to gold nanomaterials, the size of this mini-enzyme (radius of gyration ≈ 1 nm, compared to HRP ≈ 3 nm)[53] grants the possibility of drastically influencing the specific activity of functionalized nanomaterials, by increasing the active-site density.

In this work, the immobilization of the artificial peroxidase FeMC6*a on AuNPs has been exploited as a means of improving LFiA sensitivity. In particular, we describe the development of a two-step LFiA for the detection of human-IgG as a model analyte (Figure 1B), using AuNPs doubly decorated with anti-human-IgG antibodies and FeMC6*a (**Figure 2**A). The conversion of the TMB chromogen, catalyzed by FeMC6*a (Figure 2B), darkens the test line color thus increasing the LFiA sensitivity. To the best of our knowledge, this is the first proof-of-concept example of using an artificial enzyme in LFiAs. The benefits and signal enhancement properties obtained when substituting natural enzymes with FeMC6*a are discussed.

Taken together, our results demonstrate that miniaturized peptide-based artificial enzymes might be exploited in practical applications and open new perspectives in the development of diagnostic devices. Indeed, the possibility of modulating FeMC6*a behaviors by design may offer great opportunities in the optimization of LFiAs.

2. Results and Discussion

2.1. Preparation and Characterization of the AuNPs Decorated with Enzymes and Antibodies

The AuNPs were prepared following the Turkevich method,[54] by reducing tetrachloroauric acid ($HAuCl_4$) in the presence of trisodium citrate (Na_3-citrate). The citrate-stabilized AuNPs were uniform in size and shape (average diameter of 15.9 ± 0.8 nm), and highly monodisperse as ascertained by TEM analysis (Figure S1, Supporting Information). AuNPs were subsequently functionalized by adsorbing FeMC6*a and the goat anti-human-IgG antibody as dAb (Figure 2A), for analyte detection. Human-IgG was selected as the target analyte because its detection in lateral flow assays has been very well characterized and developed, both by us[4,35,55] and other groups.[56,57] This makes human-IgG an ideal analyte for testing and validating new sensing technologies, such as that based on the artificial miniaturized peroxidase FeMC6*a used in this work. Further, human-IgG detection and quantification are also clinically relevant, for the diagnosis and progression monitoring of infections.[58]

Several interdependent parameters have to be optimized to prepare biomolecule-functionalized AuNPs suitable for incorporation into lateral flow strips.[4] One of these parameters is the minimum concentration of the dAb/enzyme mixture necessary to completely cover the AuNP surface and to stabilize the colloid. Furthermore, as biomolecule adsorption onto AuNPs occurs through electrostatic and/or hydrophobic interactions, the pH greatly influences the physisorption as well as the colloidal stability. Thus, screening for optimal conditions to avoid aggregation of the AuNP-biomolecule conjugates is first needed. Subsequently, blocking agents should be used to cover the AuNPs surface area not filled with the biomolecules as well as to prevent nonspecific adsorption in the final test.

Therefore, salt-induced gold aggregation tests were performed to select the optimal conditions to functionalize AuNPs with the dAb and FeMC6*a (see Experimental Section and Figures S2–S5, Supporting Information). The ratio between the dAb and FeMC6*a was set at 9:1 (expressed in µg mL^{-1}), in order to introduce the catalytic peroxidase functionality onto AuNPs while keeping a high density of dAb on the gold surface for efficient analyte recognition. Bovine serum albumin (BSA) is the most commonly used blocking agent in LFAs but was not used in this instance, since the blocking
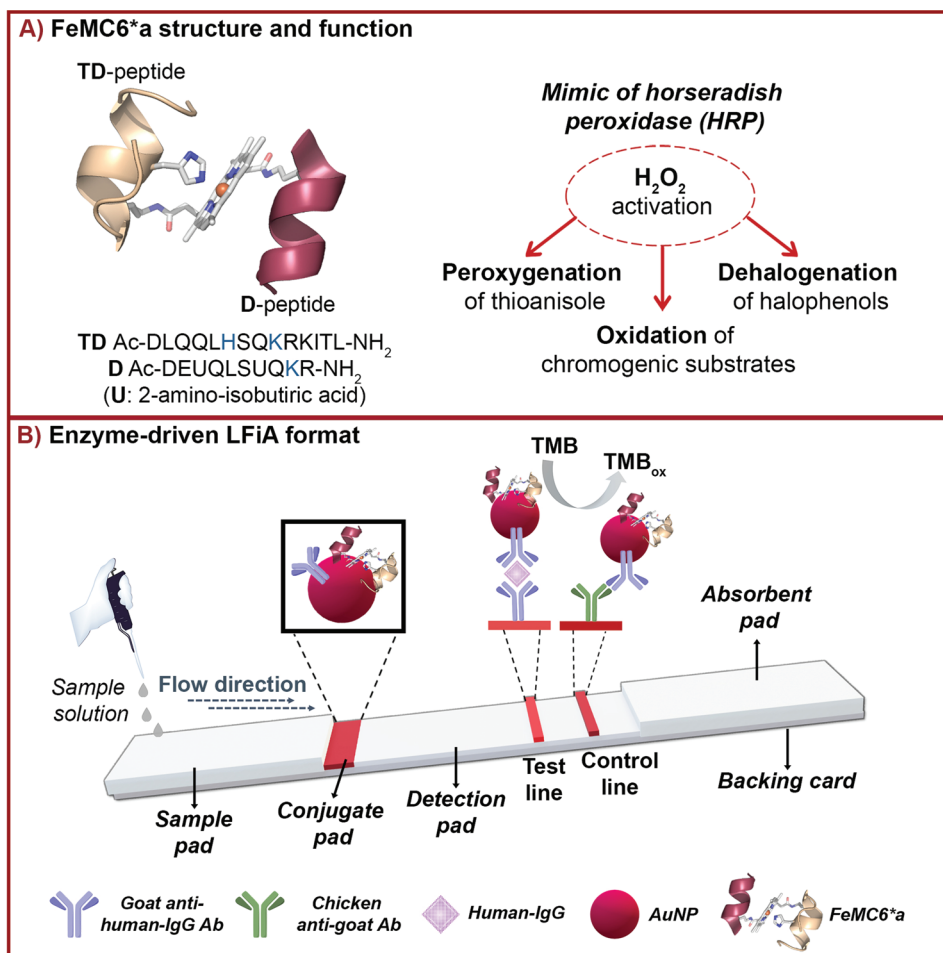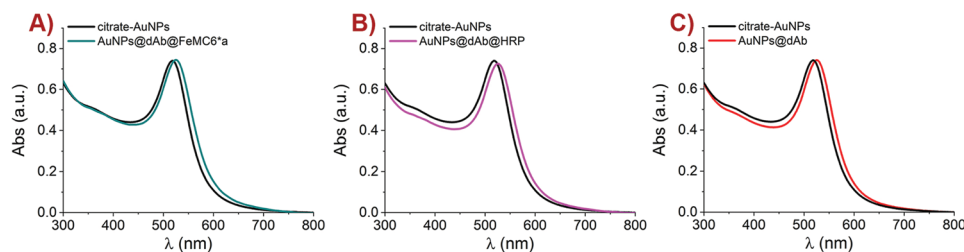
Figure 1. A) Structure of FeMC6*a obtained using PyMOL software, primary sequences of the tetradeca and deca peptides, and summary of the reactions catalyzed. B) Schematic representation (not to scale) of FeMC6*a–assisted lateral flow two-step immunoassay for human-IgG detection.

agent should be smaller than the biomolecules immobilized on AuNPs.[4] Considering that FeMC6*a is a low molecular weight peptide-porphyrin conjugate (radius of gyration ≈ 1 nm, M_W ≈ 4 kDa), poly(ethylene glycol) average M_n 400 Da
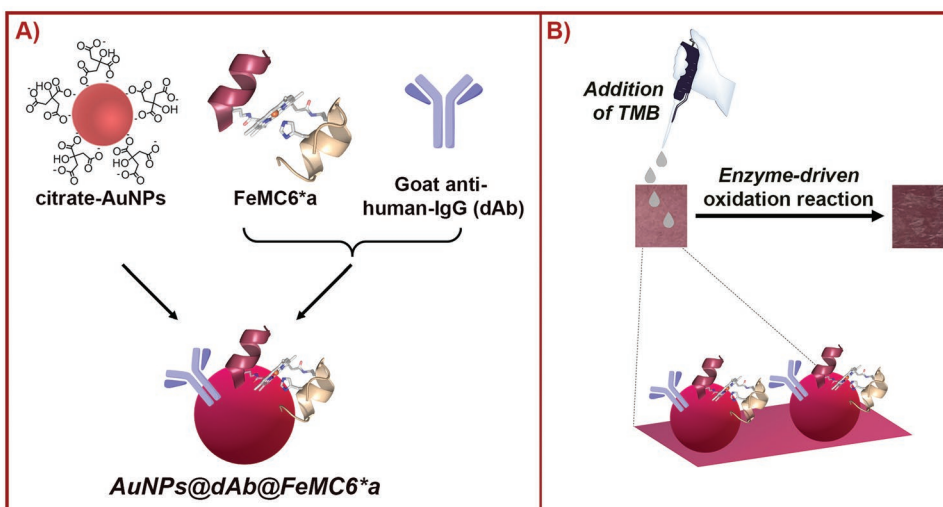
Figure 2. A) Schematic representation of the doubly decorated AuNPs, namely AuNPs@dAb@FeMC6*a, used in the LFiA. B) Changes in the color of a section of the conjugate pad, occurring in the second step of the assay format thanks to FeMC6*a-catalyzed TMB oxidation.

**ADVANCED
SCIENCE NEWS**

www.advancedsciencenews.com

NANO · MICRO

small

www.small-journal.com

Figure 3. UV–Vis spectra of citrate-AuNPs (black line) and purified, functionalized AuNPs: A) AuNPs@dAb@FeMC6*a, dark cyan line; B) AuNPs@dAb@HRP, purple line; C) AuNPs@dAb, red line.

(PEG-400) was judged to be more suitable since its dimensions are comparable to those of the miniaturized enzyme.[59] Based on the results of the gold aggregation screening, the minimum dAb/FeMC6*a concentration that gave the highest absorbance difference was 6.5 µg of biomolecules in 1 mL of the AuNPs stock solution (0.65 µg of FeMC6*a and 5.85 µg of dAb), backfilled with a 1% (v/v) aqueous solution of PEG-400 at pH 7 (Figure S5, Supporting Information).

For comparative purposes, the same conditions were used to functionalize AuNPs with goat anti-human-IgG antibodies and HRP, as well as AuNPs with only goat anti-human-IgG antibodies.

The functionalized AuNPs were then purified by centrifugation and resuspension in the conjugate pad buffer (PBS 10 mM pH 7.4, 5% w/v sucrose, 1% v/v PEG-400, 0.5% v/v Tween-20). The AuNPs were stable under these conditions, as evidenced by the absorption spectra, which showed no broadening of the surface plasmon resonance band (SPRB), nor any shift in the absorption maximum. **Figure 3** shows the UV–Vis spectra of the functionalized AuNPs, namely AuNPs@dAb@FeMC6*a, AuNPs@dAb@HRP, and AuNPs@dAb.

For all the systems, a red-shift of 6 nm in the SPRB of the citrate-stabilized AuNPs (from 520 to 526 nm) was observed after functionalization. This finding is consistent with changes in the refractive index on the surface of the nanoparticles, caused by biomolecule adsorption.[60]

TEM images of AuNPs@dAb@FeMC6*a, AuNPs@dAb@HRP and AuNPs@dAb, analyzed after negative staining with the UranyLess reagent, exhibited a white halo surrounding the gold core, evidence of the presence of a protein shell (**Figure 4**).[51,52]

After biomolecule conjugation, the size of the AuNP gold core was retained, thus evidencing the colloidal stability of the functionalized AuNPs. Some clustering, visible in the TEM images, was attributed to the deposition and drying process when preparing the samples on the carbon-coated copper grids for TEM analysis.[61] This is supported by the UV–Vis spectra of all the conjugates, where no aggregate formation could be observed (Figure 3). The average diameters of the nanoconjugates were measured as 20 ± 2 nm for AuNPs@dAb, 19.8 ± 1.3 nm for AuNPs@dAb@FeMC6*a, and 26 ± 3 nm for AuNPs@dAb@HRP, indicating that the dAb alone and together with HRP and FeMC6*a are decorating the AuNPs surface (Figure 4).

2.2. Evaluation of FeMC6*a Stability/Activity under Operational Conditions

As described above, FeMC6*a is a promiscuous, artificial miniaturized peroxidase.[44,50] The reduced size of this catalyst

compared to natural peroxidases, coupled with the easy scale-up of its synthetic route, offers significant advantages for a variety of practical applications.[49,52] To evaluate its potential as a substitute for natural enzymes in LFiA technology, its catalytic activity toward the H_2O_2-mediated TMB oxidation was assayed. Indeed, TMB plays an important role as a chromogenic substrate in HRP-based immunoassays and has also recently been defined as "the chosen substrate" in colorimetric assays, for its analytical performances as well as molecular properties, affording high sensitivity and stability.[62]
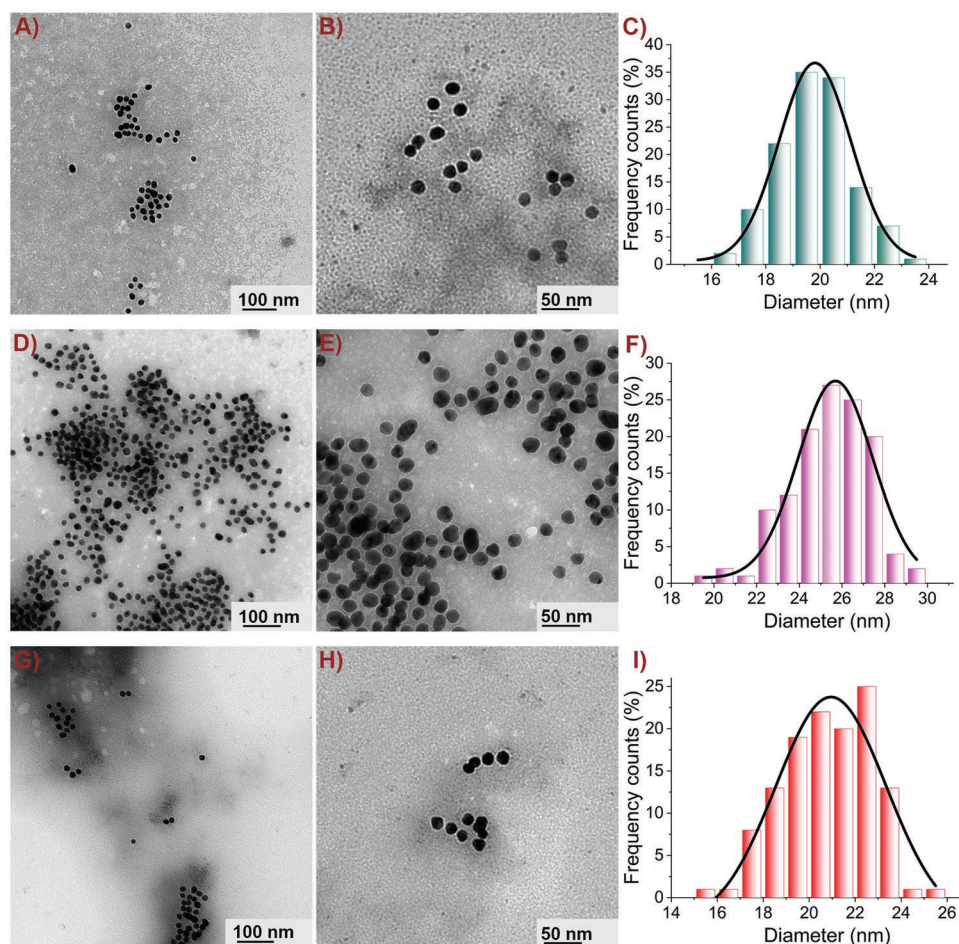
Kinetic parameters for the H_2O_2-dependent TMB oxidation catalyzed by FeMC6*a were evaluated and compared to literature data on HRP[63] (see Paragraph S3, Figure S6, and Table S1, Supporting Information). FeMC6*a and HRP showed similar turnover frequencies (k_{cat} 2600 and 3300 s^{-1}, respectively) toward TMB oxidation. However, because of the increase in TMB K_m value, FeMC6*a catalytic efficiency ($k_{cat} K_m^{-1}$) showed a 4-fold decrease when compared to the natural counterpart. Nevertheless, this finding was not considered detrimental to the assay, as it would be counterbalanced by the increase of the active site density of the immobilized enzyme on AuNPs, thanks to the reduced size of FeMC6*a with respect to HRP.

One key and critical aspect to employ enzymes in LFiAs is that the catalysts retain their function after drying and rewetting.[4] Therefore, the stability of the AuNPs@dAb@FeMC6*a was evaluated by drop casting the solution onto a conjugate pad, which was dried under vacuum (Figure 2B) and rewet. The drying process did not cause the AuNPs to aggregate (the conjugate pad did not turn a purplish color) and, most importantly, did not affect the catalytic activity of FeMC6*a. By simply adding TMB solution to the pad, rewet with PBS, it was possible to observe the change of color from reddish to dark purple, thus evidencing the successful oxidation of the chromogen substrate, catalyzed by the artificial FeMC6*a peroxidase.

2.3. Performance of the Assay using FeMC6*a and Evaluation of the Analytical Sensitivity

To assess the performance of the artificial FeMC6*a peroxidase in LFiAs, strips were prepared following a protocol established in the literature (see Experimental Section).[4,35] The assay format consists of two separate human-IgG detection events (see Figure 1B). In the first assay step, red bands at the test and control lines of the strips arise from the accumulation of AuNPs, as is typical in conventional AuNP-based LFiAs. In the second assay step, the TMB substrate was added, which is

**ADVANCED
SCIENCE NEWS**
www.advancedsciencenews.com

NANO · MICRO
small
www.small-journal.com

Figure 4. TEM images of the AuNPs-biomolecule conjugates, along with the corresponding size distribution histograms: A–C) AuNPs@dAb@FeMC6*a, D–F) AuNPs@dAb@HRP, and G–I) AuNPs@dAb. The samples were stained with UranyLess solution before observation (N ≈ 150).

oxidized by the peroxidase immobilized on AuNPs, an event expected to improve the colorimetric signal intensity. After the assembling of the strips with AuNPs@dAb@FeMC6*a, the first detection was obtained by adding a solution of human-IgG on the sample pad, allowing the solution to flow, and waiting for 15 min to see the appearance of the colorimetric signal at TL and CL. All the experiments were performed in triplicate, for a series of different analyte concentrations (see Experimental Section). Images of the lateral flow strips, with different human-IgG concentrations (between 0 and 1000 ng mL^{-1}), obtained after the first assay step are provided in **Figure 5**A. As expected, a colored test line appeared in all the positive samples, but not in the blank. The color intensity increased with the concentration of the target, and the lowest analyte concentration that produced a colored line clearly distinguishable from the blank by the naked eye was 30 ng mL^{-1} (Figure 5A).

The second step of the assay was carried out by adding 10 µL of a TMB-containing solution directly onto the lines. A commercially available, ready-to-use TMB solution was used to keep the LFiA as simple as possible, avoiding the preparation of separate solutions of substrate and oxidant. Figure 5B shows photographs of the strips after TMB addition. Comparing the

photographs in Figure 5A,B, even with the naked eye, there is a clear enhancement of the signal after TMB addition.

This is most clearly seen when examining the TL of the 10 ng mL^{-1} human-IgG, where a response is undoubtedly seen after the second step (Figure 5B) that was not present after the first step (Figure 5A). Quantitative analysis of the strips was performed by acquiring images of the strips with a scanner, and analyzing the strips using "ImageJ" (see Paragraph S4 and Figure S7, Supporting Information).[64] From the analysis of the strips, test line values were derived for the first and the second step of the assay (Figure S8, Supporting Information). The derived test line values, background subtracted, were used to evaluate the limit of detection (LoD), taking into account: i) the values obtained from the blank (LoB), ii) the standard deviation (σ) related to the blank, and iii) the values coming from the lowest concentration of human-IgG (10 ng ml^{-1}), according to the following relations: LoB = (mean value)$_{blank}$ + 3σ_{blank}; LoD = LoB + 3$\sigma_{lowest \ human-IgG \ concentration}$.[65]

Next, test line values were plotted against the target analyte concentration, for both the first and second steps of the assay (Figure 5C,D, respectively). Data fitting with a non-linear Langmuir isotherm (Equation (1) in Experimental Section) allowed the determination of the LoD as a function of the analyte

ADVANCED
SCIENCE NEWS
www.advancedsciencenews.com

NANO · MICRO
small
www.small-journal.com
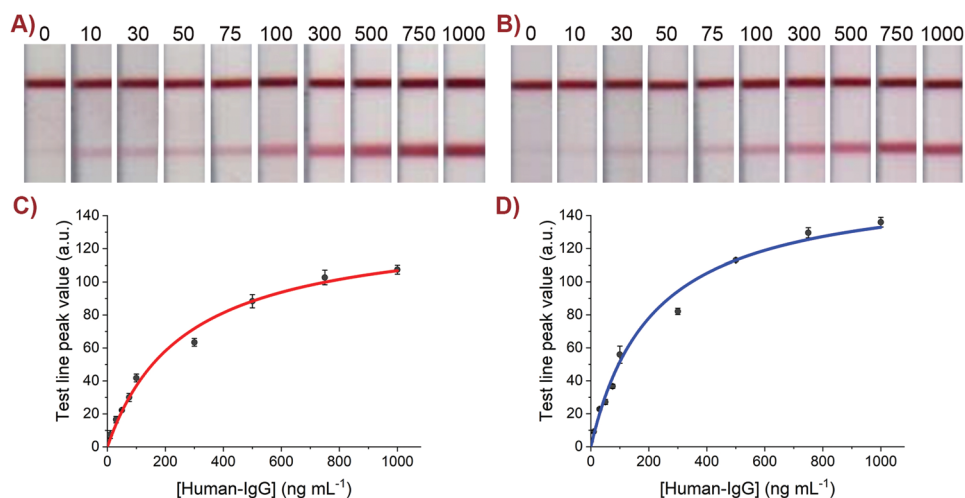
Figure 5. LFiA using AuNPs@dAb@FeMC6*a conjugates. Photographs of the strips and assay calibration curves for human-IgG detection acquired A,C) before and B,D) after the addition of the TMB solution, taken with a scanner. All concentrations were repeated in triplicate.

concentration. Prior to TMB addition, an LoD of 36.4 ± 1.4 ng mL^{-1} was determined (**Table 1**). Enhancement of the test line intensity after TMB addition was clearly evidenced by comparing the curves in Figure 5C,D. Data analysis for the second assay step, after TMB oxidation on the strips, showed that the LoD improved to 8.2 ± 1.2 ng mL^{-1} (Table 1).

2.4. Performance of the LFiA: Comparison with a Conventional Assay and when using the HRP-Containing Conjugate

The performances of the LFiAs when using AuNPs@dAb@FeMC6*a were compared with those based on AuNPs@dAb and AuNPs@dAb@HRP conjugates. The conventional LFiA, performed with strips prepared using AuNPs@dAb only (Figure S9, Supporting Information), exhibited a limit of detection of 30.5 ± 1.9 ng mL^{-1} (analysis of the strips is shown in Figure S10, Supporting Information).

Figure 6 shows photographs of the lateral flow strips prepared with AuNPs@dAb@HRP conjugates, obtained in a two-step assay format identical to that performed with FeMC6*a. As observed for the artificial peroxidase, HRP oxidation of TMB provides an enhancement of the colorimetric signal at the TL (Figure 6A,B). The LoD of the first step was found to be 37.4 ± 1.6 and 18.2 ± 0.9 ng mL^{-1} for the second step (after TMB addition), (Figure 6C,D respectively). Analysis of the strips is shown in Figure S11, Supporting Information.

The LoD values obtained in all the assay formats are compiled in Table 1. Comparing these values, it can be concluded that the presence of the enzymes, either FeMC6*a or HRP, caused a very slight decrease in the performance of the conventional assay (step 1). This is most probably a result of reducing the total amount of dAb on the nanoparticles, thereby slightly decreasing their probability of binding to the target analyte.

Interestingly, the lowest LoD value was obtained in the two-step assay format, exploiting the catalytic activity of FeMC6*a. This artificial peroxidase gave a higher than four-fold sensitivity enhancement, whereas a two-fold enhancement was observed with HRP. Such a difference in assay sensitivity may be related
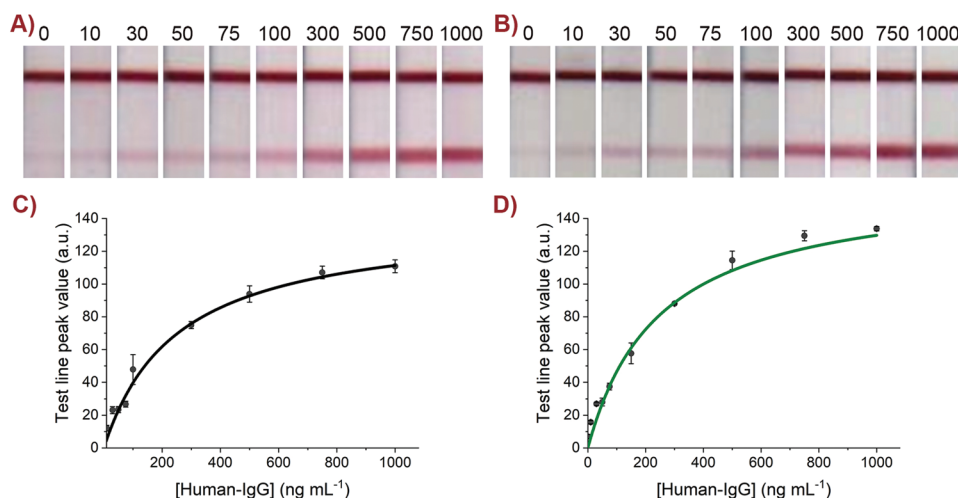
to the differences in size between the two peroxidases. The reduced size of the artificial peroxidase allows the immobilization of a higher number of active sites on the AuNPs surface. This, in turn, enhances the specific activity of AuNPs@dAb@FeMC6*a conjugate in TMB oxidation and signal amplification.

To validate this hypothesis, the amount of peroxidase (either FeMC6*a or HRP) in the AuNPs@dAb@FeMC6*a and AuNPs@dAb@HRP conjugates was estimated by quantifying the heme content, following the method reported by Onoda et al.[66] In this protocol, the AuNPs are treated with potassium cyanide (KCN), which quenches the SPRB as a consequence of converting the Au^0 to $Au^{III}(CN)_4^-$, and yields the bis-cyanide complex of the heme-containing catalyst, characterized by an absorption band at 416 nm. Using a known molar extinction coefficient, it was possible to estimate the enzyme concentration from the UV–Vis spectra. Through this procedure (see Experimental Section), the concentration of FeMC6*a in the AuNPs@dAb@FeMC6* sample was estimated to be 1.6×10^{-7} M (see Figure S12, Supporting Information). However, when the identical procedure was performed on the AuNPs@dAb@HRP conjugate, no absorbance peak was observed, highlighting that the amount of HRP in the sample was not spectroscopically detectable, and thus lower than that of FeMC6*a in the corresponding conjugate sample.

Finally, the LoD obtained with the FeMC6*a-based LFiA (8.2 ± 1.2 ng mL^{-1}) is within the range observed for signal-amplified LFiAs (usually ranging from 0.1 µg mL^{-1} to 0.1 pg mL^{-1}, as reported by Liu et al.[26]). Further, our assay shows good

Table 1. Limit of detection (LoD) values using the different systems on the conjugate pad. LoD values are reported as mean values $\pm$ SD ($n = 3$).

Label on conjugate release pad	Limit of detection [ng mL^{-1}]	
	Conventional assay	Two-step assay (TMB oxidation)
AuNPs@dAb	30.5 ± 1.9	–
AuNPs@dAb@FeMC6*a	36.4 ± 1.4	8.2 ± 1.2
AuNPs@dAb@HRP	37.4 ± 1.6	18.2 ± 0.9

**ADVANCED
SCIENCE NEWS**
www.advancedsciencenews.com

NANO · MICRO
small
www.small-journal.com

Figure 6. LFiA using AuNPs@dAb@HRP conjugate. Photographs of the strips and assay calibration curves for human-IgG detection acquired A,C) before and B,D) after the addition of the TMB solution, images recorded with a scanner. All concentrations were repeated in triplicate.

correlation with other analytical methods to detect human-IgG. LoD values reported for conventional ELISA methods for IgG quantification range from 1.6 ng mL^{-1}[67] down to 0.24 ng mL^{-1}, as claimed in a commercial kit.[68] More recently, a variety of different platforms for human-IgG detection have been reported, such as molecular imprinted SPR chips[69] or optical sensors,[70,71] achieving LoDs of 56,[69] 37,[70] and 28 ng mL^{-1}.[71]

2.5. Stability Tests

To evaluate the long-term stability of the lateral-flow strips, tests were performed by storing the strips at room temperature for 4 weeks. The detection of human-IgG at three different concentrations (0, 50, and 500 ng mL^{-1}) was carried out in triplicate on days 0, 3, 7, 15, and 30. The strips retained excellent performance for the first 7 days, whereas the optical signal decreased by 20% starting from day 15 (Figure S13, Supporting Information). This result was observed right after the first step of the assay, the recognition of human-IgG from the antibody molecules. Interestingly, the test line peak value, obtained upon the addition of TMB solution, showed that FeMC6*a copies on AuNPs retained their activity over the entire month tested. Similar results were obtained by the strips containing HRP-functionalized AuNPs (Figure S14, Supporting Information).

These data suggest that the observed decrease in the optical signal is not related to enzyme inactivation, either FeMC6*a or HRP, but to other factors, for example, loss of dAbs recognition ability over time, probably because of the presence of some surfactants (such as Tween-20), used when preparing lateral flow strips to improve the flow across the paper or the release of the label particles. Also, the presence of other proteins included on the strips (such as BSA employed as a blocking agent in nitrocellulose), could have had a detrimental effect on the stability of the strips.[4] Coefficients of variation (CVs) were calculated from the ratio of the standard deviation to the average signal. As reported in Table S2, Supporting Information, the CV values for concentrations of human-IgG ranged from 5% to 30% for the

strips containing both AuNPs@dAb@FeMC6*a and AuNPs@dAb@HRP in the conjugate pad, thus indicating good stability.

3. Conclusion

In this work, we have reported the integration of the synthetic mini-enzyme FeMC6*a into an LFiA device for the sensitive detection of human-IgG. The enzymatic reaction catalyzed by FeMC6*a exposed on the AuNPs surface allows the oxidation of TMB substrate, which in turn enhances the sensitivity of the LFiA with respect to the direct measurement of the AuNPs as non-modified optical labels. All the results reported herein prove that FeMC6*a i) tolerates the harsh conditions necessary for creating the conjugate pad of a lateral flow strip; ii) does not interfere with the binding between human-IgG and the detection/capture antibodies; iii) acts as an efficient catalyst on paper, boosting the sensitivity of the enzyme-based LFiA up to 4-fold with respect to a conventional LFiA. In fact, when using FeMC6*a as label, the visual detection limits lowered from $\approx$ 40 to $\approx$ 10 ng mL^{-1}, thus demonstrating an enhancement in sensitivity. Remarkably, when compared to its natural counterpart (HRP), FeMC6*a grants the assay with a significantly better limit of detection. Finally, the shelf-life analysis revealed that FeMC6*a functionalized strips are stable for up to a month at room temperature.

These encouraging results will inspire future optimization to assay the performance of the FeMC6*a-based LFiAs in real-world samples. Currently, the LFiA format has been developed and tested in idealized laboratory conditions and buffers to get a fundamental comparison of the performance of FeMC6*a with respect to HRP, thus highlighting the advantages of using the artificial enzyme. However, complex real-world samples (such as blood, saliva, urine, and so on) contain a plethora of biomolecules that can non-specifically bind to the lateral flow assay components and interfere with its performance. Several factors, such as the specificity of the capture and detection antibodies, coupled with the correct selection of membrane type and any necessary coatings to reduce non-specific adsorption,

ADVANCED
SCIENCE NEWS
www.advancedsciencenews.com

NANO · MICRO
small
www.small-journal.com

need to be optimized when working on real samples. Such optimization is beyond the scope of this work and will be the subject of future investigations.

Altogether, these results highlight that the reduced size of FeMC6*a with respect to HRP, coupled with the easy scale-up of its synthetic route, offers significant advantages for use in the construction of bioinspired sensors and nanomaterials. Traditionally, catalytic methods of signal enhancement in lateral flow assays have utilized chemical catalysts, enzymes and bioengineered enzymes. Moreover, very recently some nanomaterials, namely nanozymes,[72,73] have been reported as an alternative solution.

To the best of our knowledge, this is the first study presenting the implementation of a peptide-based artificial enzyme to enhance the colorimetric signal in an LFiA. Despite significant achievements reached in the field of artificial metalloenzymes, practical application in catalysis, biotechnology and sensor technology is still in their infancy. Whilst the performance enhancement achieved is not groundbreaking with respect to the obtained LoD, we believe that the introduction of a catalytic signal enhancement, through the use of a totally synthetic artificial enzyme, is of interest to the field. The added value of using an artificial enzyme like FeMC6*a, as a valuable alternative with respect to native or mutated enzymes, lies in its intrinsic characteristics, and in particular in allowing to 1) introduce new features and/or improve performance by expanding the range of amino acids beyond those used in Nature; 2) analyze the effect of mutation on recognition and catalytic activity on smaller and thus easier to study systems; 3) increase the active-site density, because of its smaller dimensions respect to native enzymes. This last point is crucial especially for applications involving enzyme immobilization, as this mini-enzyme allows a drastic increase of the specific activity of functionalized nanomaterials.

FeMC6*a has also several advantages with respect to the nanozymes that mimic HRP activity. As recently highlighted by Ashrafi et al.,[72] even though some nanozymes show interesting catalytic behaviors, they suffer from being highly variable as a result of their means of preparation. Shape, size, and polydispersity may severely change as a consequence of different experimental conditions, thus affecting their catalytic behaviors. The artificial miniaturized peroxidase FeMC6*a holds sufficient molecular behavior to replicate native enzyme function, within a defined and predetermined molecular structure. Thus, it represents a middle ground between engineered enzymes and nanozymes.

In conclusion, this work is intended as a proof-of-concept and will hopefully inspire the future optimization and development of novel Mimochromes which may further enhance the performance of lateral flow assays in real-world samples. This will allow moving away toward assay formats where the response can be enhanced by the intelligent design of artificial enzymes.

4. Experimental Section

Instruments: The test line and the control line were dispensed on the nitrocellulose membrane using an IsoFlow Bioreagent dispenser from Imagene Technology (Hanover, Germany). The functionalized nanoparticles were purified by centrifugation with an Allegra 64R from Beckman Coulter (Brea, CA, USA). The strips were cut with a lateral flow strip cutter from Shanghai Kinbio Tech (Pudong New District, Shanghai, China). The UV–Vis spectra were recorded with a SpectraMax ID3 spectrophotometer from Molecular Devices (San Jose, CA, USA), and with a Cary 60 spectrophotometer (Agilent, CA, USA) using quartz cuvettes with 1.00 cm path lengths. Wavelength scans were performed at 25 °C from 200 to 800 nm, with a 600 nm min^{-1} scan speed. All data were blank corrected. Transmission electron microscopy (TEM) micrographs were acquired in bright field mode using a TEM TECNAI G2 20ST (Fei, Hillsboro, OR, USA) operating at 120 kV. Data analysis was performed with Origin Pro 9.0 software (Origin Lab Corporation, Northampton, MA, USA), and ImageJ software (National Institutes of Health, available free of charge at Web site rsb.info.nih.gov/ij/). All the molecular graphics pictures were generated with PyMOL software (DeLano Scientific Ltd), and ChemDraw Ultra 12.

Materials and Reagents: Polyclonal goat anti-human-IgG antibody (I1886), human-IgG whole molecule (12 511), bovine serum albumin (BSA), tetrachloroauric acid solution (HAuCl$_4$, 30% w/w), trisodium citrate dihydrate (Na$_3$-citrate), phosphate buffer saline (PBS) tablets, sodium tetraborate, boric acid, sucrose, Tween-20, sodium dodecyl sulfate (SDS), and TMB ready-to-use solution (T0565) were purchased from Sigma Aldrich (Madrid, Spain). Chicken anti-goat antibody was purchased from Abcam (ab86245, Cambridge, UK). Polyclonal goat anti-human-IgG antibody was used as the detection antibody (dAb) and capture antibody on the TL, while chicken anti-goat antibody was used as a capture antibody on the CL. Poly(ethylene glycol) average M_n 400 Da (PEG-400) was purchased from Fluka. 2,2,2-trifluoroethanol (TFE) was supplied by Romil (Cambridge, UK). H$_2$O$_2$ solution (50% v/v) was provided by Merck Life Science. 3,3',5,5'-tetramethilbenzidine (TMB) was purchased from Fluka. Peroxidase from horseradish (HRP, P8375-2KU) was purchased as a lyophilized powder from Sigma Aldrich (Madrid, Spain).

The artificial protein FeMC6*a was synthesized as reported in the literature.[44]

Nitrocellulose membrane (CN150, 1UN15WR100025NT) was purchased from Sartorius Stediem (Göttingen, Germany) and used as the detection pad. Cellulose membranes (CFSP001700) were used as sample and absorbent pads and glass fiber (Standard 14, GFCP00900) was used as the conjugate pad. Both were purchased from Millipore Corporation (Billerica, MA, USA). Adhesive backing cards (MIBA-020) were purchased from DCN Dx (Carlsbad, CA, USA). Milli-Q water, produced using a Milli-Q system (18.2 MΩ cm^{-1}) purchased from Millipore (Sweden), was used for the preparation of all the solutions.

For TEM measurements, copper grids with carbon films (Ted Pella, product 08144-F, 400 mesh) were used and the nanoconjugate samples were stained with UranyLess staining solution purchased from Electron Microscopy Sciences (Hatfield, PA, USA).

Unless otherwise stated, the PBS solution (10 mM, pH 7.4) consisted of phosphate buffer(0.01 M), NaCl (0.137 M), and KCl (0.003 M). The sample pad buffer was made up of PBS containing BSA (5% w/v) and Tween-20 (0.05% v/v). The conjugate pad buffer was prepared with PBS, sucrose (5% w/v), PEG-400 (1% v/v), and Tween-20 (0.5% v/v). The washing solution contained PBS (5 mM pH 7.4) and SDS (0.01% w/v).

Synthesis and Characterization of Citrate-AuNPs: Citrate-capped gold nanoparticles were prepared following the Turkevich method.[54] Briefly, an aqueous solution of Na$_3$-citrate (1.25 mL, 1% w/v) was added to a boiling aqueous solution of HAuCl$_4$ (50 mL, 0.25 mM) under vigorous stirring. The addition of the reducing agent induced the formation of gold nanoparticles, evidenced by a color change from light yellow to bright red. After that, the solution was allowed to boil for an additional 10 min, under stirring, and finally to cool down to room temperature. The as-synthesized colloidal solution of citrate-AuNPs was stored at 4 °C in the dark until further use. The concentration of the citrate-AuNPs in solution was qualitatively evaluated by UV–Vis spectroscopy (Figure S1A, Supporting Information) following a method reported by Fernig et al.[74] The ratio between the maximum absorbance of the SPRB (A$_{SPRB}$) and the

**ADVANCED
SCIENCE NEWS**

www.advancedsciencenews.com

**NANO · MICRO
small**

www.small-journal.com

maximum absorbance at 450 nm (A_{450}) provides a qualitative indication of the AuNPs diameter, and hence of its molar extinction coefficient. For an A_{SPRB}/A_{450} ratio of 1.66, the diameter of the AuNPs was estimated to be $\approx$ 16 nm. From the value of A_{450} and using the calculated extinction coefficient (ε^{450}) of 2.67×10^8 M^{-1} cm^{-1}, the citrate-stabilized AuNP concentration in the stock solution was estimated to be 1.67 nM.

Salt-Induced Gold Aggregation Tests: During this screening, several parameters were taken into account: i) the pH of the AuNP solution, ii) the concentration and composition of the biomolecule mixture (containing goat anti-human-IgG antibody as dAb and FeMC6*a), iii) the addition of a blocking agent, and iv) the concentration of the blocking agent. The pH of citrate-AuNPs solution was adjusted until 7, 8, and 9 using borate buffer (100 mM, pH 9.2). Then, aliquots of citrate-AuNPs at the chosen pHs (150 μL) were incubated with aqueous solutions of dAb and FeMC6*a at several concentrations (10 μL, concentrations: 200, 175, 150, 125, 100, 80, 60, 40, and 0 μg mL^{-1}, of which 10% was FeMC6*a and 90% was dAb). After that, the blocking process was performed using an aqueous solution of PEG-400 (10 μL; 0, 1, 2, and 3% v/v) and the test ended with the addition of a solution of NaCl (20 μL, 10% w/v). Each step was carried out for 20 min at 25 °C, 650 rpm. Finally, UV–Vis spectra were recorded, and the degree of aggregation was measured by the red-shift of the SPR bands relative to the 520 nm value obtained from the stable solution of citrate-AuNPs (Figures S2–S4, Supporting Information). The difference between the absorbance at 520 nm and at 580 nm (taken as the absorbance value for aggregated AuNPs) was evaluated and plotted against the concentration used (Figure S5A–C, Supporting Information).[75]

Functionalization of AuNPs: The physisorption of goat anti-human-IgG antibody (dAb) and FeMC6*a on AuNPs was performed as follows, using the optimal conditions elucidated by the gold aggregation tests and referring to some procedures reported in the literature.[76,77] Prior to this procedure, separate stock solutions of dAb and FeMC6*a (2.0 mg mL^{-1}) were prepared in Milli-Q water. Then, a solution containing both the biomolecules (600 μL, 110 μg mL^{-1} in Milli-Q water containing 6.6 μg of FeMC6*a and 59.4 μg of dAb) was added to an AuNP solution (9.0 mL, pH 7 adjusted with borate buffer 100 mM, pH 9.2) at 650 rpm and 25 °C for 90 min. To this, a solution of PEG-400 (600 μL, 1% v/v in Milli-Q water) was added and incubated under the same conditions for 30 min. The sample of functionalized AuNPs was then purified by centrifugation (10 000 rpm, 40 min, 4 °C). After that, the clear supernatant was discarded and the collected pellet was re-suspended in 3.0 mL of the conjugate pad buffer, to afford AuNPs@dAb@FeMC6*a. The same synthetic and purification procedures were performed using HRP (stock solution 2.0 mg mL^{-1} in Milli-Q water) instead of FeMC6*a, to give AuNPs@dAb@HRP.

Likewise, the AuNPs@dAb sample was prepared by incubating the AuNPs solution (9.0 mL) with the goat anti-human-IgG antibody solution (600 μL, 110 μg mL^{-1} in Milli-Q water) and incubated at 650 rpm and 25 °C for 30 min. Next, a solution of PEG-400 (600 μL, 1% v/v in Milli-Q water) was added to the mixture and incubated at the same conditions. After that, the excess reagents were removed by centrifugation (10 000 rpm, 30 min, 4 °C) and the collected precipitate was dispersed in 3.0 mL of the conjugate pad buffer.

After purification, UV–Vis spectra were acquired by diluting the sample three times with the conjugate pad buffer (Figure 3). No broadening of the bands or loss of nanomaterial was observed, as the absorbance values recorded are the same as those of citrate-AuNPs, indicating that the concentration of AuNPs in the undiluted stock solutions is $\approx$ 5 nM for AuNPs@dAb@FeMC6*a, AuNPs@dAb@HRP, and AuNPs@dAb.

Characterization of Functionalized AuNP Samples: Transmission electron microscopy (TEM) micrographs were acquired in bright field mode. The samples for TEM analyses were prepared by loading the functionalized AuNP solutions (5 μL) onto carbon-coated copper grids for 10 min and removing the excess solution with filter paper. High negative contrast, to visualize the biomolecular shell around AuNPs, was afforded with UranyLess staining solution. The staining solution (5 μL) was deposited on the grid and the staining procedure was performed for

2 min. After that, the excess solution was removed with filter paper, and the grid was rinsed with Milli-Q water. The grids were allowed to air-dry at room temperature overnight.[78]

Fabrication of the Strips: The printing of the test and control lines on the nitrocellulose membrane (CN150) was performed with a bioreagent dispenser using goat anti-human-IgG (1 mg mL^{-1} in phosphate buffer 10 mM, pH 7.4) and chicken to goat antibody (1 mg mL^{-1} in phosphate buffer 10 mM, pH 7.4) respectively. The lines were then dried in the oven at 37 °C for 2 h. After drying, the nitrocellulose membrane was blocked with a solution of BSA (2% w/v) in PBS for 20 min and washed two times using the washing solution (15 min, two times). The conjugate pad was prepared by dispensing the conjugate solution, containing either AuNPs@dAb@FeMC6*a, AuNPs@dAb@HRP or AuNPs@dAb, depending on the selected format assays, on the glass fiber and drying it in a vacuum chamber at room temperature for 2 h. The sample pads were pre-treated by soaking the cellulose membrane in the sample pad buffer and dried in the oven at 37 °C for 3 h. Finally, the assembling of the pads was guided by laminated cards, already containing the nitrocellulose membranes, and cut into 0.3 cm-width strips with a lateral flow cutter. The size of the strips was fixed at 6 × 0.3 cm, with a bed volume of 90 μL.

Procedure of the Assay: The assay was conceived to be performed in two steps: i) the appearance of the CL and TL because of the flow of human-IgG solutions on the LFiA strips; ii) the addition of TMB solution on the colored lines. For the first step, solutions of human-IgG (90 μL, concentrations 0, 10, 30, 50, 75, 100, 300, 500, 750, and 1000 ng mL^{-1}, prepared in PBS) were dispensed on the sample pad. PBS without an analyte was used as a blank. All the measurements were carried out in triplicate.

The solution was allowed to reach the absorbent pad and the strips were left under ambient conditions for 15 min to allow the lines to develop. Then, the strips were washed with PBS (70 μL) to improve the background color. For the second step, the ready-to-use solution of the chromogen TMB was added directly to the test line and the control line (10 μL) and a period of time of 10 min was waited to allow the oxidative conversion of the chromogenic substrate. An enhancement of the red color of the lines was ascertained by the naked eye. After each step, images of the strips were acquired using a SkanMulti LFA scanner and the quantitative data analysis was performed with ImageJ software, in order to construct calibration curves. Details about the analysis of the strips are given in the Supporting Information (Figures S7, S8, S10, and S11, Supporting Information).

Each set of data points was fitted to the non-linear Langmuir isotherm equation. This model initially devised to describe the adsorption behavior of gaseous molecules to a solid substrate as a function of gas pressure, is now widely exploited for the quantification of the number of molecular adsorbates on a solid substrate as a function of the concentration of the molecule in solution.[79,80] In this case, the solid-liquid interaction between the capture antibody on the test line and the antigen bound to the detection antibody (carried along the strip by AuNPs) could be modeled. From previous studies, it was known that there was a 1:1 stoichiometric binding ratio between the antibody and the human-IgG. The following equation was used:

$$\theta = \frac{\theta_m K [Human-IgG]}{1 + K [Human-IgG]} \tag{1}$$

where θ is the fraction of human-IgG molecules bound by goat anti-human-IgG antibody (the capture antibody on the test line); θ_m is the maximum number of bound human-IgG molecules; [Human-IgG] is the concentration of analyte in ng mL^{-1}, and K is the Langmuir constant, which is a parameter indicating the strength of the interaction between the antibody and the antigen. θ is related to the test line optical value evaluated with ImageJ (background subtracted) and θ_m is the test line optical value related to the highest concentration of human-IgG.

Evaluation of the Iron Content with Cyanide Method: Iron content in AuNPs@dAb@FeMC6*a and AuNPs@dAb@HRP conjugate samples was evaluated as reported in the literature.[66] The procedure was based

on the disruption of the gold core and the consequent formation of a bis-cyanide-heme complex of the heme-containing peroxidases (FeMC6*a and HRP). The absorbance of this complex was directly proportional to the concentration of heme, thus of the enzyme in the conjugate sample. The molar extinction coefficient for the bis-cyanide-heme complex formed with FeMC6*a was first evaluated by performing cyanide binding experiments. In detail, a stock solution of FeMC6*a ($3.5~\mu L$, 1.1×10^{-3} M in H_2O 0.1% v/v TFA) was mixed with a stock aqueous solution of KCN (196.5 μL, 2.5×10^{-5} or 2.5×10^{-2} M, pH 12). The addition of a 1.25-fold molar excess of cyanide ions led to the mono-cyanide adduct with the ferric heme of the artificial enzyme, which Soret band was positioned at 406 nm (Figure S12A, Supporting Information, blue line).[81] On the contrary, the addition of a 125-fold molar excess of KCN gave rise to the bis-cyanide-heme adduct, with a Soret band at 416 nm and a single Q band at 550 nm (Figure S12A, Supporting Information, purple line), as similar UV–Vis response was observed for the bis-cyanide complex of natural heme-proteins.[82] The absorption of the bis-cyanide-heme adduct was employed to evaluate the value of the molar extinction coefficient at 416 nm ($\varepsilon^{416} = 61\ 754$ M^{-1} cm^{-1}). Regarding the experiment with the conjugate samples, aliquots of AuNPs@dAb@FeMC6*a and AuNPs@dAb@HRP (750 μL each) were concentrated by centrifugation (10 000 rpm, 30 min, 4 °C) and the collected precipitate (20 μL) was treated with an aqueous solution of KCN (80 μL, 2.5×10^{-2} M). After an incubation time of 20 min, to allow the disintegration of the gold core, UV–Vis spectra were recorded and the absorption at 416 nm was used to evaluate the iron content in the conjugates. The experiments were repeated in triplicate.

Stability Assay: The stability assay was carried out at room temperature. The strips were stored under Ar, in sealed bags in the dark. The detection of human-IgG, before and after the addition of TMB solution, was performed on days 0, 3, 5, 7, and 30 using solutions of analyte at three different concentrations (0, 50, and 500 ng mL^{-1} in PBS). The images of the strips were taken with a SkanMulti LFA scanner and the optical intensity of the test line was evaluated with ImageJ software. The results of the stability assays are given in the supporting information (Figures S13 and S14, Supporting Information).

Statistical Analysis: The evaluated LoD values are reported as mean values ± SD, considering three repetitions ($n = 3$).

Data analysis was performed with Origin Pro 9.0 software. Analysis of the images was carried out using ImageJ software.

Supporting Information

Supporting Information is available from the Wiley Online Library or from the author.

Conflict of Interest

The authors declare no conflict of interest.

Data Availability Statement

The data that support the findings of this study are available from the corresponding author upon reasonable request.

[1] C. Parolo, A. Merkoçi, *Chem. Soc. Rev.* **2013**, *42*, 450.

[2] S. Sharma, J. Zapatero-Rodríguez, P. Estrela, R. O'Kennedy, *Biosensors* **2015**, *5*, 577.

[3] K. M. Koczula, A. Gallotta, *Essays Biochem.* **2016**, *60*, 111.

[4] C. Parolo, A. Sena-Torralba, J. F. Bergua, E. Calucho, C. Fuentes-Chust, L. Hu, L. Rivas, R. Álvarez-Diduk, E. P. Nguyen, S. Cinti, D. Quesada-González, A. Merkoçi, *Nat. Protoc.* **2020**, *15*, 3788.

[5] D. Quesada-González, A. Merkoçi, *Biosens. Bioelectron.* **2015**, *73*, 47.

[6] A. Sena-Torralba, R. Álvarez-Diduk, C. Parolo, A. Piper, A. Merkoçi, *Chem. Rev.* **2022**, *122*, 14881.

[7] B. Khlebtsov, N. Khlebtsov, *Nanotechnology* **2008**, *19*, 435703.

[8] W. Ren, D. R. Ballou, R. FitzGerald, J. Irudayaraj, *Biosens. Bioelectron.* **2019**, *126*, 324.

[9] F. Di Nardo, M. Chiarello, S. Cavalera, C. Baggiani, L. Anfossi, *Sensors* **2021**, *21*, 5185.

[10] A.-C. Mirica, D. Stan, I.-C. Chelcea, C. M. Mihailescu, A. Ofiteru, L.-A. Bocancia-Mateescu, *Front. Bioeng. Biotechnol.* **2022**, *10*, 922772.

[11] E. Calucho, C. Parolo, L. Rivas, R. Álvarez-Diduk, A. Merkoçi, in *Comprehensive Analytical Chemistry* (Ed: A. Merkoçi), Elsevier, Amsterdam, The Netherlands **2020**, Ch. 10.

[12] W. C. Mak, V. Beni, A. P. F. Turner, *TrAC, Trends Anal. Chem.* **2016**, *79*, 297.

[13] A. E. Urusov, A. V. Zherdev, B. B. Dzantiev, *Biosensors* **2019**, *9*, 89.

[14] J. Park, *Sensors* **2022**, *22*, 7398.

[15] Pregnancy Tests, Clearblue, https://uk.clearblue.com/pregnancy-tests (accessed: October **2022**).

[16] B. D. Grant, C. E. Anderson, J. R. Williford, L. F. Alonzo, V. A. Glukhova, D. S. Boyle, B. H. Weigl, K. P. Nichols, *Anal. Chem.* **2020**, *92*, 11305.

[17] W. W.-W. Hsiao, T.-N. Le, D. M. Pham, H.-H. Ko, H.-C. Chang, C.-C. Lee, N. Sharma, C.-K. Lee, W.-H. Chiang, *Biosensors* **2021**, *11*, 295.

[18] J. Heskin, S. J. C. Pallett, A. Al-Hindawi, G. W. Davies, M. Rayment, N. Mughal, P. Randell, R. Jones, L. S. P. Moore, *Sci. Rep.* **2022**, *12*, 8811.

[19] D. Quesada-González, G. A. Jairo, R. C. Blake, D. A. Blake, A. Merkoçi, *Sci. Rep.* **2018**, *8*, 16157.

[20] H. Sohrabi, M. R. Majidi, M. Fakhraei, A. Jahanban-Esfahlan, M. Hejazi, F. Oroojalian, B. Baradaran, M. Tohidast, M. de la Guardia, A. Mokhtarzadeh, *Talanta* **2022**, *243*, 123330.

[21] B. K. Van Weemen, A. H. W. M. Schuurs, *FEBS Lett.* **1971**, *15*, 232.

[22] G. A. Posthuma-Trumpie, J. Korf, A. van Amerongen, *Anal. Bioanal. Chem.* **2009**, *393*, 569.

[23] H. Ye, X. Xia, *J. Mater. Chem. B* **2018**, *6*, 7102.

[24] J. D. Bishop, H. V. Hsieh, D. J. Gasperino, B. H. Weigl, *Lab Chip* **2019**, *19*, 2486.

[25] Y. Kim, J. Gonzales, Y. Zheng, *Small* **2021**, *17*, 2004988.

ADVANCED
SCIENCE NEWS
www.advancedsciencenews.com

NANO · MICRO
small
www.small-journal.com

[26] Y. Liu, L. Zhan, Z. Qin, J. Sackrison, J. C. Bischof, *ACS Nano* **2021**, *15*, 3593.

[27] W. Kim, S. Lee, S. Jeon, *Sens. Actuators, B* **2018**, *273*, 1323.

[28] Z. Gao, H. Ye, D. Tang, J. Tao, S. Habibi, A. Minerick, D. Tang, X. Xia, *Nano Lett.* **2017**, *17*, 5572.

[29] C. N. Loynachan, M. R. Thomas, E. R. Gray, D. A. Richards, J. Kim, B. S. Miller, J. C. Brookes, S. Agarwal, V. Chudasama, R. A. McKendry, M. M. Stevens, *ACS Nano* **2018**, *12*, 279.

[30] C. Parolo, M. Medina-Sánchez, A. de la Escosura-Muñiz, A. Merkoçi, *Lab Chip* **2013**, *13*, 386.

[31] S. Liu, X. Luo, R. Shu, Y. Liao, L. Dou, T. Bu, S. Wang, Y. Li, J. Sun, D. Zhang, M. Zhu, J. Wang, *Small* **2022**, *18*, 2204859.

[32] L. Rivas, M. Medina-Sánchez, A. de la Escosura-Muñiz, A. Merkoçi, *Lab Chip* **2014**, *14*, 4406.

[33] A. Sena-Torralba, D. B. Ngo, C. Parolo, L. Hu, R. Álvarez-Diduk, J. F. Bergua, G. Rosati, W. Surareungchai, A. Merkoçi, *Biosens. Bioelectron.* **2020**, *168*, 112559.

[34] D. Calabria, M. M. Calabretta, M. Zangheri, E. Marchegiani, I. Trozzi, M. Guardigli, E. Michelini, F. Di Nardo, L. Anfossi, C. Baggiani, M. Mirasoli, *Sensors* **2021**, *21*, 3358.

[35] C. Parolo, A. de la Escosura-Muñiz, A. Merkoçi, *Biosens. Bioelectron.* **2013**, *40*, 412.

[36] F. Nastri, M. Chino, O. Maglio, A. Bhagi-Damodaran, Y. Lu, A. Lombardi, *Chem. Soc. Rev.* **2016**, *45*, 5020.

[37] L. Leone, M. Chino, F. Nastri, O. Maglio, V. Pavone, A. Lombardi, *Biotechnol. Appl. Biochem.* **2020**, *67*, 495.

[38] K. J. Koebke, T. Kühl, E. Lojou, B. Demeler, B. Schoepp-Cothenet, O. Iranzo, V. L. Pecoraro, A. Ivancich, *Angew. Chem., Int. Ed.* **2021**, *60*, 3974.

[39] M. J. Chalkley, S. I. Mann, W. F. DeGrado, *Nat. Rev. Chem.* **2021**, *6*, 31.

[40] K. J. Koebke, T. B. J. Pinter, W. C. Pitts, V. L. Pecoraro, *Chem. Rev.* **2022**, *122*, 12046.

[41] M. Chino, L. Leone, G. Zambrano, F. Pirro, D. D'Alonzo, V. Firpo, D. Aref, L. Lista, O. Maglio, F. Nastri, A. Lombardi, *Biopolymers* **2018**, *109*, 23107.

[42] F. Nastri, D. D'Alonzo, L. Leone, G. Zambrano, V. Pavone, A. Lombardi, *Trends Biochem. Sci.* **2019**, *44*, 1022.

[43] F. Nastri, L. Lista, P. Ringhieri, R. Vitale, M. Faiella, C. Andreozzi, P. Travascio, O. Maglio, A. Lombardi, V. Pavone, *Chemistry* **2011**, *17*, 4444.

[44] G. Caserta, M. Chino, V. Firpo, G. Zambrano, L. Leone, D. D'Alonzo, F. Nastri, O. Maglio, V. Pavone, A. Lombardi, *ChemBioChem* **2018**, *19*, 1823.

[45] V. Firpo, J. M. Le, V. Pavone, A. Lombardi, K. L. Bren, *Chem. Sci.* **2018**, *9*, 8582.

[46] E. H. Edwards, J. M. Le, A. A. Salamatian, N. L. Peluso, L. Leone, A. Lombardi, K. L. Bren, *J. Inorg. Biochem.* **2022**, *230*, 111753.

[47] L. Leone, D. D'Alonzo, V. Balland, G. Zambrano, M. Chino, F. Nastri, O. Maglio, V. Pavone, A. Lombardi, *Front. Chem.* **2018**, *6*, 590.

[48] L. Leone, D. D'Alonzo, O. Maglio, V. Pavone, F. Nastri, A. Lombardi, *ACS Catal.* **2021**, *11*, 9407.

[49] G. Zambrano, F. Nastri, V. Pavone, A. Lombardi, M. Chino, *Sensors* **2020**, *20*, 3793.

[50] G. Zambrano, A. Sekretareva, D. D'Alonzo, L. Leone, V. Pavone, A. Lombardi, F. Nastri, *RSC Adv.* **2022**, *12*, 12947.

[51] G. Zambrano, E. Ruggiero, A. Malafronte, M. Chino, O. Maglio, V. Pavone, F. Nastri, A. Lombardi, *Int. J. Mol. Sci.* **2018**, *19*, 2896.

[52] G. Zambrano, M. Chino, E. Renzi, R. Di Girolamo, O. Maglio, V. Pavone, A. Lombardi, F. Nastri, *Biotechnol. Appl. Biochem.* **2020**, *67*, 549.

[53] F. Auriemma, C. De Rosa, A. Malafronte, R. Di Girolamo, C. Santillo, Y. Gerelli, G. Fragneto, R. Barker, V. Pavone, O. Maglio, A. Lombardi, *ACS Appl. Mater. Interfaces* **2017**, *9*, 29318.

[54] J. Turkevich, P. C. Stevenson, J. Hillier, *Discuss. Faraday Soc.* **1951**, *11*, 55.

[55] G. E. Nunes Pauli, A. de la Escosura-Muñiz, C. Parolo, I. H. Bechtold, A. Merkoçi, *Lab Chip* **2015**, *15*, 399.

[56] N. Alam, L. Tong, Z. He, R. Tang, L. Ahsan, Y. Ni, *Cellulose* **2021**, *28*, 8641.

[57] J. Jeon, S. H. Lee, Y. Joung, K. Kim, N. Choi, J. Choo, *Sens. Actuators, B* **2020**, *321*, 128521.

[58] A. Ivanov, E. Semenova, *J. Med. Virol.* **2021**, *93*, 5953.

[59] C. J. Fee, J. M. Van Alstine, *Bioconjugate Chem.* **2004**, *15*, 1304.

[60] A. C. Templeton, J. J. Pietron, R. W. Murray, P. Mulvaney, *J. Phys. Chem. B* **2000**, *104*, 564.

[61] B. Michen, C. Geers, D. Vanhecke, C. Endes, B. Rothen-Rutishauser, S. Balog, A. Petri-Fink, *Sci. Rep.* **2015**, *5*, 9793.

[62] X. Zhang, Q. Yang, Y. Lang, X. Jiang, P. Wu, *Anal. Chem.* **2020**, *92*, 12400.

[63] Y. Ni, J. Li, Z. Huang, K. He, J. Zhuang, W. Yang, *J. Nanopart. Res.* **2013**, *15*, 2038.

[64] C. A. Schneider, W. S. Rasband, K. W. Eliceiri, *Nat. Methods* **2012**, *9*, 671.

[65] D. A. Armbruster, T. Pry, *Clin. Biochem. Rev.* **2008**, *29*, S49.

[66] A. Onoda, Y. Ueya, T. Sakamoto, T. Uematsu, T. Hayashi, *Chem. Commun.* **2010**, *46*, 9107.

[67] S. Wang, Z. Chen, J. Choo, L. Chen, *Anal. Bioanal. Chem.* **2016**, *408*, 1015.

[68] Invitrogen: IgG (Total) Human ELISA Kit, https://www.thermofisher. com/elisa/product/BMS2091TEN.html (accessed: January **2023**).

[69] G. Ertürk, L. Uzun, M. A. Tümer, R. Say, A. Denizli, *Biosens. Bioelectron.* **2011**, *28*, 97.

[70] J. P. Mendes, L. C. C. Coelho, P. A. S. Jorge, C. M. Pereira, *Biosensors* **2022**, *12*, 515.

[71] H. Liu, Y. Sun, J. Guo, W. Liu, L. Liu, Y. Meng, X. Yu, *IEEE Access* **2021**, *9*, 116286.

[72] A. M. Ashrafi, Z. Bytesnikova, J. Barek, L. Richtera, V. Adam, *Biosens. Bioelectron.* **2021**, *192*, 113494.

[73] P. Mishra, J. Lee, D. Kumar, R. O. Louro, N. Costa, D. Pathania, S. Kumar, J. Lee, L. Singh, *Adv. Funct. Mater.* **2022**, *32*, 2108650.

[74] W. Haiss, N. T. K. Thanh, J. Aveyard, D. G. Fernig, *Anal. Chem.* **2007**, *79*, 4215.

[75] A. Ambrosi, F. Airò, A. Merkoçi, *Anal. Chem.* **2010**, *82*, 1151.

[76] P. Ciaurriz, F. Fernández, E. Tellechea, J. F. Moran, A. C. Asensio, *Beilstein J. Nanotechnol.* **2017**, *8*, 244.

[77] Z. Zhang, Y. Liu, C. Zhang, W. Luan, *Toxicon* **2015**, *96*, 89.

[78] M. Rames, Y. Yu, G. Ren, *J. Vis. Exp.* **2014**, *90*, 51087.

[79] J. D. Andrade, V. Hlady, in *Biopolymers/Non-Exclusion HPLC* (Eds.: H. Benoit, H.-J. Cantow, G. Dall'Asta, K. Dušek, H. Fujita, M. Gordon, G. Henrici-Olivé, G. Heublein, H. Höcker, H.-H. Kausch, J. P. Kennedy, A. Ledwith, S. Okamura, S. Olivé, C. G. Overberger, H. Ringsdorf, T. Saegusa, J. L. Schrag, G. V. Schulz, W. P. Slichter), Vol. *79*, Springer, Berlin **1986**, Ch. 6.

[80] S. Sohn, D. Kim, *Chemosphere* **2005**, *58*, 115.

[81] O. Maglio, M. Chino, C. Vicari, V. Pavone, R. O. Louro, A. Lombardi, *Chem. Commun.* **2021**, *57*, 990.

[82] J. Dybas, T. Chiura, K. M. Marzec, P. J. Mak, *J. Phys. Chem. B* **2021**, *125*, 3556.